

# Influences of accreting primordial black holes on the global 21 cm signal in the dark ages

Yupeng Yang <sup>\*</sup>

*School of Physics and Physical Engineering, Qufu Normal University, Qufu, Shandong, 273165, China*

3 February 2022

## ABSTRACT

Baryonic matter can be accreted onto primordial black holes (PBHs) formed in the early Universe. The radiation from accreting PBHs is capable of altering the evolution of the intergalactic medium (IGM), leaving marks on the global 21 cm signal in the dark ages. For accreting PBHs with mass  $M_{\text{PBH}} = 10^3(10^4) M_{\odot}$  and mass fraction  $f_{\text{PBH}} = 10^{-1}(10^{-3})$ , the brightness temperature deviation  $\Delta\delta T_b$  reaches  $\sim 18$  (26) mK at redshift  $z \sim 90$  ( $\nu \sim 16$  MHz), and the gradient of the brightness temperature  $d\delta T_b/d\nu$  reaches  $\sim 0.8$  (0.5) mK MHz<sup>-1</sup> at frequency  $\nu \sim 28$  MHz ( $z \sim 50$ ). For larger PBHs with higher mass fraction, the brightness temperature deviation is larger in the redshift range  $z \sim 30$ – $300$  ( $\nu \sim 5$ – $46$  MHz), and the gradient is lower at the frequency range  $\nu \sim 20$ – $60$  MHz ( $z \sim 23$ – $70$ ). It is impossible to detect these low frequency radio signals from the Earth due to the influences of the Earth’s ionosphere. However, after taking care of the essential factors properly e.g. the foreground and interference, future radio telescope in lunar orbit or on the farside surface of the Moon has a chance to detect the global 21 cm signals impacted by accreting PBHs and distinguish them from the standard model.

**Key words:** cosmology:dark matter

## 1 INTRODUCTION

As a main component of the Universe, dark matter (DM) has been confirmed by many astronomical observations, but its nature still remains mysterious (Jungman et al. 1996; Bertone et al. 2005). Many DM models have been proposed and the most studied is the weakly interacting massive particles (WIMPs). On the other hand, no detection of WIMPs has rekindled the interest in other DM models such as primordial black holes (PBHs), especially for the recent successful detection of gravitational waves caused possibly by the mergers of PBHs (Bird et al. 2016; Kohri & Terada 2021; De Luca et al. 2021a,b; Carr et al. 2020).

PBHs can form in the early Universe through the collapse of the large density perturbation. PBHs with masses  $M_{\text{PBH}} \lesssim 10^{-16} M_{\odot}$  can emit different kinds of particles via the Hawking radiation (Carr et al. 2010; Page 1977, 1976b,a). Due to the interactions between the particles emitted from PBHs and the particles existed in the Universe, the evolution of the intergalactic medium (IGM) can be changed through the effects of ionizing, heating, and excitation. PBHs with masses  $M_{\text{PBH}} \gtrsim 10 M_{\odot}$  can also radiate high energy photons in the process of accreting baryonic

matter onto them, and these radiations can also affect the evolution of IGM. The changes of the evolution of IGM will be reflected in relevant astronomical observations, such as the anisotropy of cosmic microwave background (CMB) and the global 21 cm signal (Yang 2019, 2018; Clark et al. 2018; Ricotti et al. 2008; Cang et al. 2021; Poulin et al. 2017; Ali-Haïmoud & Kamionkowski 2017; Tashiro & Sugiyama 2013).

Recently, the Experiment to Detect the Global Epoch of Reionization Signature (EDGES) reported the observation of the global 21 cm signal, showing an absorption feature with an amplitude  $T_{21} \sim 500$  mK centered at redshift  $z \sim 17$ . The maximum amplitude observed is about twice larger than expected (Bowman et al. 2018; Xu et al. 2021; Villanueva-Domingo et al. 2020; Cohen et al. 2017). The abnormal signal could be explained by many different schemes (Barkana 2018; Feng & Holder 2018; Yang 2018). On the other hand, the observational results of EDGES can be used to investigate the properties of DM (Clark et al. 2018; D’Amico et al. 2018; Yang 2018; Kovetz et al. 2019; Bhatt et al. 2019; Berlin et al. 2018; Barkana et al. 2018; Jia & Liao 2019; Hektor et al. 2018; Mittal et al. 2021). The influence caused by the Hawking radiation from PBHs on the evolution of IGM has been investigated, and then the constraints on the abundance of PBHs has been ob-

\* Contact e-mail: [ypyang@aliyun.com](mailto:ypyang@aliyun.com)

tained utilizing the EDGES results for  $M_{\text{PBH}} \sim 10^{15} - 10^{17}$  g (Clark et al. 2018). PBHs with masses  $M_{\text{PBH}} \sim 10^{13} - 10^{14}$  g, whose lifetime is smaller than the present age of the Universe, have evaporated in the redshift range  $z \sim 6 - 1100$ . The observational results of EDGES can also be used to put upper limits on the initial mass fraction of these short-lived PBHs (Yang 2020; Halder & Banerjee 2021).

In theory, the global 21 cm signal appears in the epochs of reionization ( $z \sim 6 - 10$ ), cosmic dawn ( $z \sim 10 - 30$ ) and dark ages ( $z \sim 30 - 300$ ) (Furlanetto et al. 2006; Pritchard & Loeb 2012). In redshift  $z \lesssim 30$ , although the radiation from PBHs can effect the global 21 cm signal, the main effects come from the standard cosmological structures. Therefore, the dark ages is the best epoch of investigating the effects of PBHs. However, the frequency of the global 21 cm signal in the dark ages is redshifted to  $\nu \lesssim 40$  MHz. The observation of these signals on the Earth is effected strongly by the Earth's ionosphere. Therefore, future radio telescopes on the Moon or the satellites around low Lunar orbit are proposed (Burns et al. 2019, 2021; Burns 2020; Chen et al. 2019). Especially for the Lunar far-side, the influences from anthropogenic radio frequency interference can be mitigated. In this paper, we investigate the influences of the radiation from accreting PBHs on the evolution of IGM and the global 21 cm signal in the dark ages. Then we discuss the possibilities of detecting accreting PBHs, combining with the expected observational ability of future experiments on the global 21 cm signal.

This paper is organized as follows. In Sec. II we discuss the basic properties of accreting PBHs. The influences of accreting PBHs on the evolution of IGM and the global 21 cm signal in the dark ages are investigated in Sec. III. The relevant discussions and conclusions are given in Sec. IV. and V., respectively.

## 2 THE BASIC PROPERTIES OF ACCRETING PBHs

The spherical accretion of matter onto a point mass has been first researched by Hoyle & Lyttleton (1939, 1940b,a); Bondi & Hoyle (1944); Bondi (1952). An accretion disk could be formed if the accretion material has non-negligible angular momentum (Shapiro & Lightman 1976; Agol & Kamionkowski 2002; Poulin et al. 2017). Here we briefly review the basic properties of spherical accretion and give the relevant discussions about disk accretion.

A PBH with mass  $M$  can accrete ambient baryonic matter at the Bondi-Hoyle rate  $\dot{M}_{\text{HB}}$ , which can be written as follows (Poulin et al. 2017)

$$\dot{M}_{\text{HB}} = 4\pi\lambda\rho_{\infty}\frac{(GM)^2}{v_{\text{eff}}^3}, \quad (1)$$

where  $G$  is the gravitational constant.  $\rho_{\infty} = n_{\infty}m_p$  is the mass density far away from the PBH.  $m_p$  is the proton mass and  $n_{\infty}$  is the mean cosmic gas density (Poulin et al. 2017; Ricotti et al. 2008)

$$n_{\infty} = 200 \text{ cm}^{-3} \left(\frac{1+z}{1000}\right)^3. \quad (2)$$

Accretion parameter  $\lambda$  takes into account the effects of gas viscosity, the Hubble expansion and the Compton scattering between the CMB and gas. Ricotti et al. (2008) has given a fitted formula of  $\lambda$  based on their analysis, which ignores the differences between low and high redshift ranges. A complete and detailed analysis is performed by Ali-Haïmoud & Kamionkowski (2017). They found a factor of  $\sim 10$  decrease for  $\lambda$  at low redshift and we adopt their relevant results for our calculations. The effective velocity  $v_{\text{eff}}$  takes into account the gas sound speed far away from PBHs and the relative velocity between PBHs and baryons. The gas sound speed  $c_{s,\infty}$  is in the form of (Poulin et al. 2017)

$$c_{s,\infty} = \sqrt{\frac{\gamma(1+x_e)T}{m_p}}, \quad (3)$$

where  $\gamma = 5/3$  and  $x_e$ ,  $T$  and  $m_p$  are the ionization fraction, the temperature of baryons, and the mass of proton, respectively. For the redshift range considered here, the gas sound speed  $c_{s,\infty}$  can be approximated as follows (Poulin et al. 2017)

$$c_{s,\infty} \approx 6 \text{ km s}^{-1} \left(\frac{1+z}{1000}\right)^{1/2}. \quad (4)$$

In the linear regime, the square root of the variance of the relative velocity  $v_L$  is (Poulin et al. 2017; Ricotti et al. 2008)

$$\langle v_L^2 \rangle^{1/2} \approx \min \left[ 1, \frac{1+z}{1000} \right] \times 30 \text{ km s}^{-1}. \quad (5)$$

In the non-linear regime ( $z \lesssim 30$ ), the relative velocity  $v_{\text{NL}}$  is different from that in the linear regime and can be approximated as  $\langle v_{\text{NL}}^2 \rangle^{1/2} \approx 620 (1+z)^{-2.3} \text{ km s}^{-1}$  (Hasinger 2020). Because we will investigate the global 21 cm signal in the dark ages, therefore, the relative velocity  $v_L$  is used for our calculations. In order to investigate the energy injected into the IGM, one should average the luminosity of PBHs over the Gaussian distribution of relative velocities (Ali-Haïmoud & Kamionkowski 2017; Poulin et al. 2017; Ricotti et al. 2008). For this case, Ali-Haïmoud & Kamionkowski (2017) have proposed that the effective velocity is in the form of  $v_{\text{eff}} \equiv \langle (c_{s,\infty}^2 + v_L^2)^{-3} \rangle^{-1/6}$  and can be approximated as follows

$$v_{\text{eff}} \approx \begin{cases} \sqrt{c_{s,\infty} \langle v_L^2 \rangle^{1/2}} & \text{for } c_{s,\infty} \ll \langle v_L^2 \rangle^{1/2} \\ c_{s,\infty} & \text{for } c_{s,\infty} \gg \langle v_L^2 \rangle^{1/2} \end{cases} \quad (6)$$

The accretion luminosity of a PBH is proportional to the Bondi-Hoyle rate  $\dot{M}_{\text{HB}}$  (Poulin et al. 2017)

$$L_{\text{acc,PBH}} = \epsilon \dot{M}_{\text{HB}} c^2, \quad (7)$$

where  $\epsilon$  is radiative efficiency. It depends on the details of accretion and a typical value is  $\epsilon = 0.01\dot{m}$  for spherical accretion (Ricotti et al. 2008). Ali-Haïmoud & Kamionkowski

(2017) reanalyzed the accretion process of PBHs and found a updated form for redshift  $z \lesssim 500$ ,

$$\frac{\epsilon}{\dot{m}} \sim \begin{cases} 10^{-3} & \text{for photoionization} \\ 10^{-5} & \text{for collisional ionization} \end{cases} \quad (8)$$

where  $\dot{m} = \dot{M}_{\text{HB}} c^2 / L_{\text{Edd}}$ ,  $L_{\text{Edd}} = 1.26 \times 10^{38} (M/M_{\odot}) \text{ erg s}^{-1}$  is the Eddington luminosity. The energy injection rate per unit volume of accreting PBHs can be written as follows (Poulin et al. 2017)

$$\left( \frac{dE}{dV dt} \right)_{\text{PBH}} = L_{\text{acc, PBH}} f_{\text{pbh}} \frac{\rho_{\text{DM}}}{M_{\text{PBH}}}, \quad (9)$$

where  $f_{\text{pbh}} = \rho_{\text{PBH}} / \rho_{\text{DM}}$ . Here we have assumed a monochromatic mass function for PBHs. For extended mass function, the energy injection rate per unit volume of accreting PBHs depends on the other parameters (Cang et al. 2021).

### 3 THE EVOLUTION OF THE IGM AND GLOBAL 21 CM SIGNAL IN THE DARK AGES INCLUDING THE INFLUENCE OF ACCRETING PBHS

#### 3.1 The evolution of the IGM including accreting PBHs

The evolution of the IGM is changed due to the effects of radiation from accreting PBHs. The main effects on the IGM are heating, ionization, and excitation (Zhang et al. 2007; Chen & Kamionkowski 2004; Clark et al. 2018; Yang 2019, 2015, 2018; Belotsky & Kirillov 2015). The changes of the ionization fraction ( $x_e$ ) and the temperature of IGM ( $T_k$ ) with redshift are governed by following equations (Yang 2019, 2015; Chen & Kamionkowski 2004; Zhang et al. 2007)

$$(1+z) \frac{dx_e}{dz} = \frac{1}{H(z)} [R_s(z) - I_s(z) - I_{\text{PBH}}(z)], \quad (10)$$

$$(1+z) \frac{dT_k}{dz} = \frac{8\sigma_T a_R T_{\text{CMB}}^4 x_e (T_k - T_{\text{CMB}})}{3m_e c H(z) (1 + f_{\text{He}} + x_e)} - \frac{2}{3k_B H(z)} \frac{K_{\text{PBH}}}{1 + f_{\text{He}} + x_e} + T_k, \quad (11)$$

where  $R_s(z)$  and  $I_s(z)$  are recombination and ionization rate respectively caused by the standard sources.  $I_{\text{PBH}}$  and  $K_{\text{PBH}}$  are the ionization and heating rate caused by accreting PBHs (Zhang et al. 2007; Chen & Kamionkowski 2004; Yang 2019; Clark et al. 2018; Yang 2015),

$$I_{\text{PBH}} = f(z) \frac{1}{n_b} \frac{1}{E_0} \times \left( \frac{dE}{dV dt} \right)_{\text{PBH}} \quad (12)$$

$$K_{\text{PBH}} = f(z) \frac{1}{n_b} \times \left( \frac{dE}{dV dt} \right)_{\text{PBH}} \quad (13)$$

where  $f(z)$  stands for the energy fraction injected into the IGM for ionization, heating, and exciting, respectively. It is a function of redshift and has been investigated detailed by e.g. Madhavacheril et al. (2014); Slatyer (2016). We

have used the public code ExoCLASS (Stöcker et al. 2018), which is a branch of the public code CLASS (Blas et al. 2011), to calculate  $f(z)$  (Poulin et al. 2017). In order to solve the differential equations mentioned above, we have followed the method used by e.g. Yang (2019, 2015, 2020); Chen & Kamionkowski (2004); Zhang et al. (2007); Clark et al. (2018), modifying the public code RECFAST in CAMB<sup>1</sup> to include the effects of radiation from accreting PBHs. The changes of  $x_e$  and  $T_k$  with redshift are shown in Fig. 1 (top and middle panels), where we also plot the fractional difference of  $x_e$  ( $T_k$ ), defined as  $\Delta x_e / x_e = (x_{e, \text{PBH}} - x_e) / x_e$ , for accreting PBHs with  $M_{\text{PBH}} = 10^3$  ( $10^4$ )  $M_{\odot}$  and  $f_{\text{PBH}} = 10^{-1}$  ( $10^{-3}$ ), respectively. For comparison, the standard case without accreting PBHs is also shown in Fig. 1 (dotted line). The top panel of Fig. 1 shows that the recombination is delayed due to the influence of accreting PBHs. At redshift  $z \sim 100$ , compared to the standard case, the ionization fraction  $x_e$  (the temperature of IGM  $T_k$ ) increases about  $\sim 150\%$  (30%) and  $\sim 300\%$  (35%) respectively for the considered models of accreting PBHs.

#### 3.2 The global 21 cm signal in the dark ages including accreting PBHs

The 21 cm line is related to the hyperfine transition between the triplet and singlet levels of the ground state of hydrogen atom. With  $n_0$  and  $n_1$  as the number densities of hydrogen atoms in triplet and singlet states, the spin temperature  $T_s$  is defined as follows (Furlanetto et al. 2006; Pritchard & Loeb 2012)

$$\frac{n_1}{n_0} = 3 \exp \left( -\frac{0.068\text{K}}{T_s} \right). \quad (14)$$

The spin temperature is influenced by the background photons, the collisions between particles, and the resonant scattering of Ly $\alpha$  photons (Wouthuysen-Field effect) (Pritchard & Loeb 2012; Furlanetto et al. 2006).  $T_s$  is related to the temperature of CMB ( $T_{\text{CMB}}$ ) and IGM ( $T_k$ ) as follows (Yuan et al. 2010; Cumberbatch et al. 2010)

$$T_s = \frac{T_{\text{CMB}} + (y_{\alpha} + y_c) T_k}{1 + y_{\alpha} + y_c}, \quad (15)$$

where  $y_{\alpha}$  corresponds to the Wouthuysen-Field effect and we use the formula (Yuan et al. 2010; Yang 2019; Kuhlen et al. 2006)

$$y_{\alpha} = \frac{P_{10}}{A_{10}} \frac{0.068\text{K}}{T_k} e^{-0.3 \times (1+z)^{0.5} T_k^{-2/3} \left(1 + \frac{0.4}{T_k}\right)^{-1}}, \quad (16)$$

where  $A_{10} = 2.85 \times 10^{-15} \text{ s}^{-1}$  is the Einstein coefficient of hyperfine spontaneous transition.  $P_{10}$  is the radiative de-excitation rate due to Ly $\alpha$  photons (Pritchard & Loeb 2012; Furlanetto et al. 2006).  $y_c$  is related to the collisions between hydrogen atoms and other particles (Yuan et al. 2010; Yang 2018; Kuhlen et al. 2006; Liszt 2001; Yang 2016),

$$y_c = \frac{(C_{\text{HH}} + C_{\text{eH}} + C_{\text{pH}}) 0.068\text{K}}{A_{10} T_k}, \quad (17)$$

<sup>1</sup> <https://camb.info/>

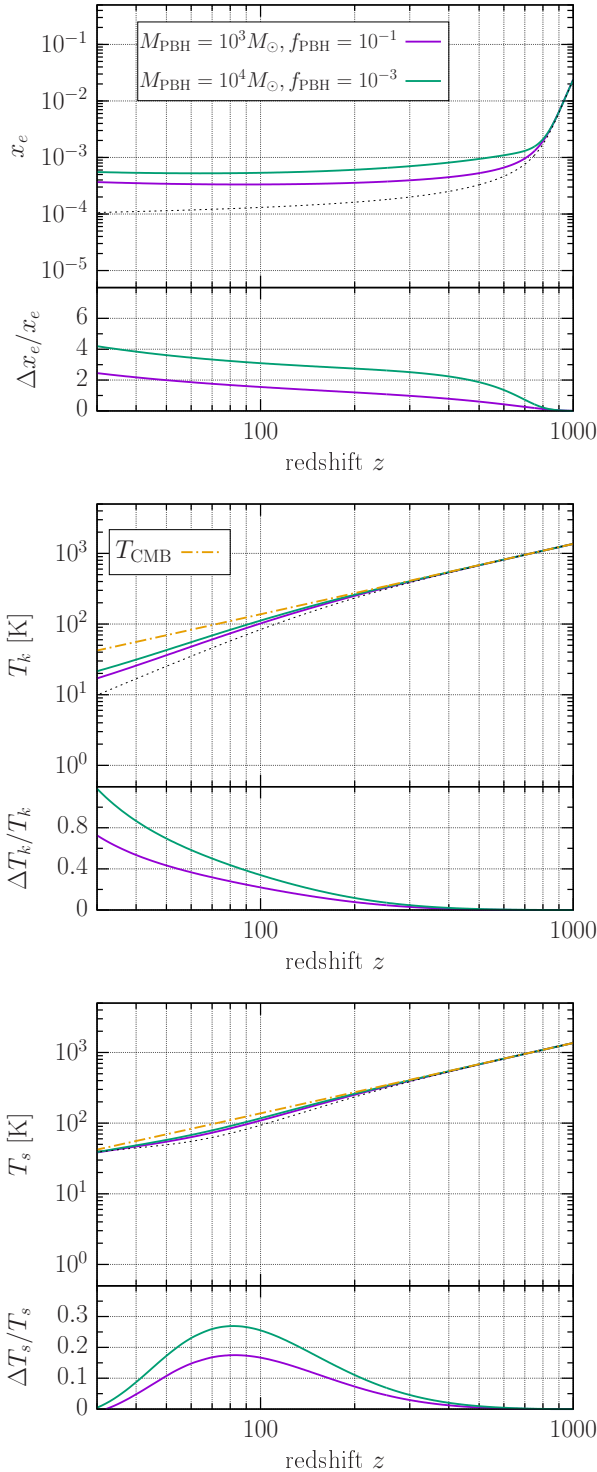


**Figure 1.** The changes of the ionization fraction ( $x_e$ , top panel), the gas temperature ( $T_k$ , middle panel), and the spin temperature ( $T_s$ , bottom panel) with redshift  $z$  for accreting PBH models with  $M_{\text{PBH}} = 10^3(10^4) M_\odot$  and  $f_{\text{PBH}} = 10^{-1}(10^{-3})$ . The dotted line stands for the standard scenario without accreting PBHs. The fractional difference of  $x_e$  is defined as  $\Delta x_e/x_e = (x_{e,\text{PBH}} - x_e)/x_e$  and the same definition is applied to  $T_k$  and  $T_s$ . Here we have set the radiative efficiency  $\epsilon = 10^{-5}\dot{m}$ , corresponding to the case of collisional ionization (Ali-Haïmoud & Kamionkowski 2017).

where  $C_{\text{HH,eH,pH}}$  are the de-excitation rate and we adopt the fitted formulas used by Yang (2018, 2016); Kuhlen et al. (2006); Liszt (2001).

The differential brightness temperature,  $\delta T_b$ , relative to the CMB can be written as follows (Cumberbatch et al. 2010; Ciardi & Madau 2003; Yang 2018)

$$\delta T_b = 26(1 - x_e) \left( \frac{\Omega_b h}{0.02} \right) \left[ \frac{1+z}{10} \frac{0.3}{\Omega_m} \right]^{\frac{1}{2}} \times \left( 1 - \frac{T_{\text{CMB}}}{T_s} \right) \text{ mK}. \quad (18)$$

The variations of the spin temperature  $T_s$  with redshift are shown in the bottom panel of Fig. 1. We also plot the fractional difference in  $T_s$ , defined as  $\Delta T_s/T_s = (T_{s,\text{PBH}} - T_s)/T_s$ , for the considered models of accreting PBHs.  $T_s$  is decoupled with  $T_{\text{CMB}}$  at redshift  $z \sim 600$  and coupled again at redshift  $z \sim 30$ . Including the influence of accreting PBHs, the maximum fractional difference appears at redshift  $z \sim 80$  and the degree of difference depends on the specific model of accreting PBHs.

In the top panel of Fig. 2, we show the evolution of the differential brightness temperature  $\delta T_b$  with redshift  $z$ . As shown in Fig. 1, compared to the standard scenario, the spin temperature  $T_s$  increases in the redshift range  $z \sim 30 - 400$  for the case of accreting PBHs. Since the differential brightness temperature  $\delta T_b$  is proportional to  $(1 - T_{\text{CMB}}/T_s)$ , the amplitude of  $\delta T_b$  is decreased as shown in Fig. 2. In addition, we also show the brightness temperature deviation,  $\Delta \delta T_b = \delta T_{b,\text{PBH}} - \delta T_b$ , of the considered accreting PBHs models from the standard scenario (dotted line). The deviation  $\Delta \delta T_b$  achieves the maximum value  $\sim 18$  (26) mK at redshift  $z \sim 90$  for accreting PBHs with  $M_{\text{PBH}} = 10^3$  ( $10^4$ )  $M_\odot$  and  $f_{\text{PBH}} = 10^{-1}$  ( $10^{-3}$ ).

The gradient of the differential brightness temperature,  $d\delta T_b/d\nu$ , is shown in the bottom panel of Fig. 2, where the dotted line stands for the standard case. For the standard case,  $d\delta T_b/d\nu$  achieves  $\sim 1.8$  mK MHz $^{-1}$  at the frequency  $\nu \sim 28$  MHz ( $z \sim 50$ ). Including the effects of accreting PBHs, in the frequency range of  $\nu \sim 20 - 40$  MHz, the amplitude of  $d\delta T_b/d\nu$  is lowered and  $\lesssim 1$  mK MHz $^{-1}$  for the considered models of accreting PBHs.

## 4 DISCUSSIONS

Since the frequency of the global 21 cm signal in the dark ages is redshifted to  $\nu \lesssim 40$  MHz and the Earth's ionosphere has a strong influence on the detection of these signals, it is impossible to detect these radio signals from the Earth. It has been proposed that the radio telescope, which is in either lunar orbit or on the farside surface of the Moon, can detect the global 21 cm signal in the dark ages (Burns et al. 2019, 2021; Burns 2020; Chen et al. 2019). Burns et al. (2019) argued that future radio telescope can detect the differential brightness temperature of the global 21 cm signal in the dark ages with  $1\sigma$  uncertainty of  $\delta T_b \sim 15$  mK, depending on the observation time. For accreting PBHs with mass  $M_{\text{PBH}} = 10^3 M_\odot$  and mass fraction  $f_{\text{PBH}} = 10^{-1}$ , the brightness temperature deviation  $\Delta \delta T_b$  reaches  $\sim 18$  mK at the frequency  $\nu \sim 16$  MHz. At the same frequency, the deviation  $\Delta \delta T_b$  is up to  $\sim 26$  mK for  $M_{\text{PBH}} = 10^4 M_\odot$  and  $f_{\text{PBH}} = 10^{-3}$ . Therefore, it is expected that future extraterrestrial radio telescope has the ability to distinguish the ac-



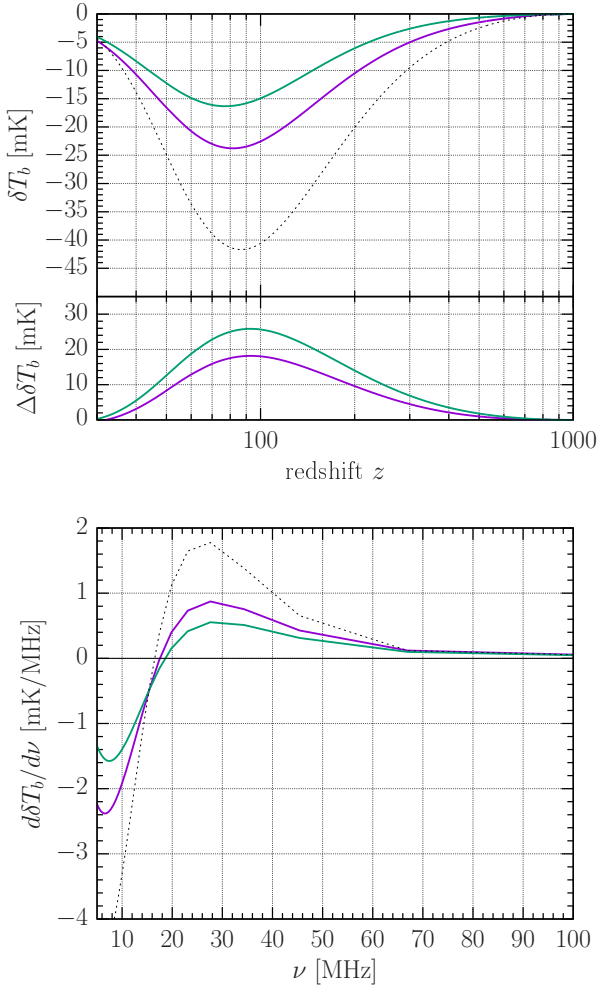


**Figure 2.** *Top panel.* The changes of the brightness temperature deviation,  $\Delta\delta T_b = \delta T_{b,\text{PBH}} - \delta T_b$ , with redshift  $z$  for accreting PBH models same as in Fig. 1. *Bottom panel.* The gradient of the differential brightness temperature  $d\delta T_b/d\nu$  as a function of frequency  $\nu$ . The line style is the same as in Fig. 1.

creting PBHs model from the standard model, especially for larger PBHs with higher mass fraction.

For the geometry of gas accretion onto PBHs, we have considered the conservative case of spherical accretion but not disk accretion. The formation of an accretion disk and its impacts on the anisotropy of CMB have been discussed by e.g. Poulin et al. (2017); Ricotti et al. (2008). A thin disk around a PBH could be formed for  $\dot{m} > 1$  and the radiative efficiency  $\epsilon$  is about  $\sim 0.06 - 0.4$  (Ricotti et al. 2008). For the scenario considered here, the accretion rate is  $\dot{m} < 1$  and a thick disk could be formed if the accreting gas has non-negligible angular momentum. In this case, an advection dominated accretion flow (Yuan & Narayan 2014) can be formed and the radiative efficiency is about a factor of ten larger than that of spherical accretion (Ricotti et al. 2008). As a result, in the disk accretion scenario  $x_e$ ,  $T_k$ , and  $T_s$  will be increased comparing to the case of spherical accretion for the same mass and mass fraction of PBHs. It is also expected that the amplitude of absorption trough ( $|\delta T_b|$ ) of the global 21 cm signal in the dark ages becomes smaller, and the brightness temperature deviation  $\Delta\delta T_b$  becomes larger

for the disk accretion scenario. In Fig. 3, the comparison between the cases of spherical accretion and disk accretion is shown for  $M_{\text{PBH}} = 10^3 M_\odot$  and  $f_{\text{PBH}} = 10^{-1}$ . For disk accretion, we have set the accretion parameter  $\lambda = 0.01$  and the radiative efficiency  $\epsilon = 0.1\dot{m}$ , corresponding to the benchmark model used by Poulin et al. (2017) for investigating the effects on the CMB. For this case, emission signals appear in the redshift range  $z \sim 30 - 100$ . The brightness temperature deviation  $\Delta\delta T_b$  reaches  $\sim 48$  mK at the frequency  $\nu \sim 18$  MHz ( $z \sim 80$ ). The gradient of the differential brightness temperature  $d\delta T_b/d\nu$  achieves  $\sim 0.8$  mK MHz $^{-1}$  at the frequency  $\nu \sim 14$  MHz ( $z \sim 100$ ).

The mass fraction of PBHs has been constrained by different astrophysical observations (for a recent review see e.g. Carr et al. (2020)). Poulin et al. (2017) have used the Planck data to get the upper limits on the mass fraction of PBHs. They found that for  $M_{\text{PBH}} = 10^3 M_\odot$  the limits are  $f_{\text{PBH}} \lesssim 10^{-2}$  ( $\lesssim 10^{-4}$ ) for spherical accretion (disk accretion). In Fig. 4, we show the brightness temperature deviation  $\Delta\delta T_b$  for different mass fraction of PBHs with  $M_{\text{PBH}} = 10^3 M_\odot$  for disk accretion. For  $f_{\text{PBH}} \sim 10^{-4}$ , the maximum deviation is  $\sim 1$  mK at redshift  $z \sim 85$  ( $\nu \sim 17$  MHz). It is smaller than  $1\sigma$  uncertainty of  $\delta T_b \sim 5$  mK, which could be achieved by  $\sim 10^5$  hours observation of future radio telescope (Burns 2020; Rapetti et al. 2020). The brightness temperature deviation  $\Delta\delta T_b$  reaches  $\sim 8$  mK at redshift  $z \sim 85$  for  $f_{\text{PBH}} \sim 10^{-3}$ . It can also be found that for  $f_{\text{PBH}} \sim \text{few} \times 10^{-3} - 10^{-2}$ , at the redshift range  $z \sim 50 - 100$ , the brightness temperature deviation can be larger than  $1\sigma$  uncertainty of  $\delta T_b \sim 15$  mK, which could be achieved by  $\sim 20000$  hours observation of future radio telescope (Burns 2020; Rapetti et al. 2020).<sup>2</sup>

In Fig. 5, the expected upper limits on  $f_{\text{PBH}}$  are shown for future detection of the global 21 cm signal in the dark ages (red solid line, labelled with dark ages). The constraints are obtained by requiring  $\delta T_b \lesssim -37$  mK, which corresponds to 5 mK uncertainty of the largest amplitude of the global 21 cm signal ( $\delta T_b \sim -42$  mK) in the dark ages. For comparison, constraints from a few other studies are also shown: 1) constraints from the global 21 cm signal in the cosmic dawn reported by the Experiment to Detect the Global Epoch of Reionization Signature (EDGES) (Hektor et al. 2018) (brown dashed line, labelled with EDGES); 2) the expected constraints from the 21 cm power spectrum in the cosmic dawn, which could be detected by e.g. the Hydrogen Epoch of Reionization Array (HERA) (Mena et al. 2019) (black dashed line, labelled with HERA); 3) upper limits from the CMB data observed by Planck (Poulin et al. 2017) (blue dashed line, labelled with Planck); 4) constraints from the studies of the effects of PBHs on the dynamical evolution of stars in dwarf galaxy Segue I (Koushiappas & Loeb 2017) (green dashed line, labelled with Segue I); 5) the non-detection of the stochastic gravitational wave background by LIGO (Raidal et al. 2017) (magenta line, labelled with LIGO); 6) constraints from the investigation of the number density of X-ray objects in galaxies (Inoue & Kusenko 2017) (orange line, labelled with X-ray). Compared with the con-

<sup>2</sup> Here we neglect the frequency dependence of uncertainty and one can refer to Rapetti et al. (2020) for more detailed discussions.

straints from LIGO, the upper limits from the dark ages are stronger for the mass range of  $300 \lesssim M_{\text{PBH}} \lesssim 10^4 M_{\odot}$ . The similar cases with a slightly different mass range can also be found for EDGES, Planck, X-ray, and Segue I. As shown in Fig. 5, future detection of the 21 cm power spectrum by e.g. HERA could provide the strongest constraints for the mass range considered here. Although the constraints from the dark ages is not the strongest, as mentioned above, since the astrophysical environment of the dark ages is relatively clean, future detection of the global 21 cm signal in the dark ages is still very useful for the studies of PBHs. Note that there are many works of investigating the constraints on the mass fraction of PBHs not shown in Fig. 5, and one can refer to e.g. Carr et al. (2020) for a recent review.

For our calculations, we have considered the gas accretion onto ‘naked’ PBHs. If PBHs did not make up all dark matter, they should also accrete dark matter particles around them forming ‘clothed’ PBHs (Ricotti et al. 2008; De Luca et al. 2020; Cai et al. 2021; Ricotti 2007). The accretion rate of ‘clothed’ PBHs is larger than ‘naked’ PBHs (Ricotti et al. 2008). Therefore, compared with the case of ‘naked’ PBHs, the brightness temperature deviation of the global 21 cm signal in the dark ages should be larger for the case of ‘clothed’ PBHs for the same mass and mass fraction of PBHs.

For the calculations above, we have set the radiative efficiency  $\epsilon = 10^{-5} \dot{m}$ , corresponding to the case of collisional ionization (Ali-Haïmoud & Kamionkowski 2017). For photoionization the radiative efficiency is about two orders of magnitude larger (Eq. 8). Therefore, the brightness temperature deviation of the global 21 cm signal in the dark ages should be larger for the case of photoionization than that of collisional ionization for the same mass and mass fraction of PBHs.

## 5 CONCLUSIONS

We have investigated the influences of accreting PBHs on the global 21 cm signal in the dark ages. By taking into account the benchmark model (spherical accretion) of accreting PBHs with mass  $M_{\text{PBH}} = 10^3$  ( $10^4$ )  $M_{\odot}$  and mass fraction  $f_{\text{PBH}} = 10^{-1}$  ( $10^{-3}$ ), we found that the maximum brightness temperature deviation of the global 21 cm signal,  $\Delta\delta T_b$ , achieve  $\sim 18$  (26) mK at redshift  $z \sim 90$ , corresponding to the frequency  $\nu \sim 16$  MHz. The gradient of the differential brightness temperature  $d\delta T_b/d\nu$  is  $\sim 0.8$  (0.5)  $\text{mK MHz}^{-1}$  for the considered models. For larger PBHs with higher mass fraction, the brightness temperature deviation is larger in the redshift range of  $z \sim 30 - 300$  ( $\nu \sim 5 - 46$  MHz) and the gradient is lower in the frequency range  $\nu \sim 20 - 40$  MHz ( $z \sim 35 - 70$ ). In addition, an accretion disk can be formed around PBHs if the accreting gas has non-negligible angular momentum. Due to the higher radiative efficiency in the disk accretion scenario, the brightness temperature deviation and the gradient of the global 21 cm signal are larger than that of spherical accretion.

Due to the influences of the Earth’s ionosphere, it is impossible to detect the global 21 cm signal in the dark ages from the Earth. Future radio telescopes in lunar orbit or on the farside surface of the Moon, where the uncertainty of detecting the brightness temperature of the global 21 cm signal

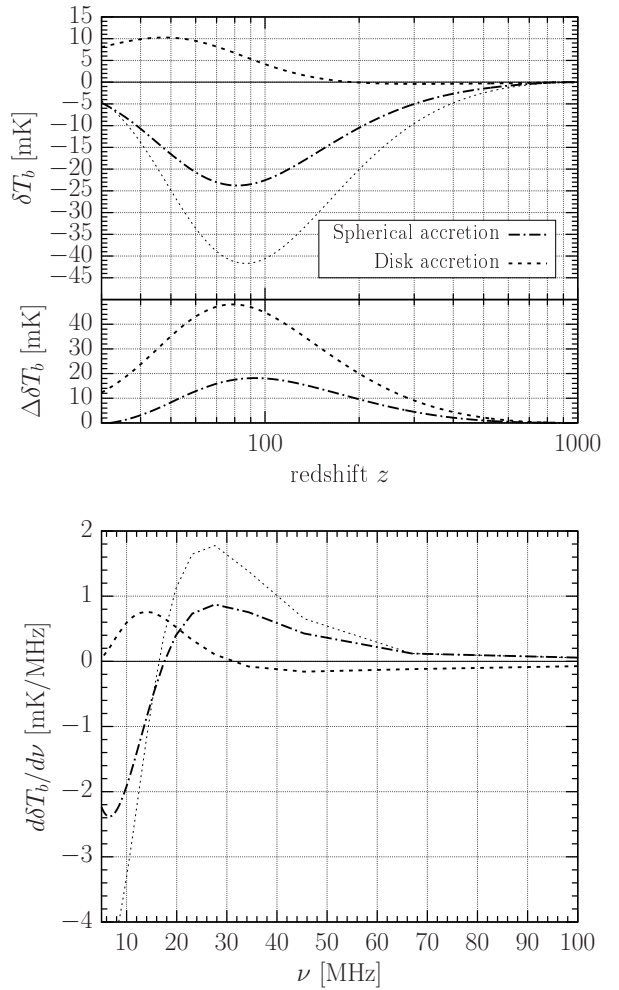


**Figure 3.** The comparison between the cases of spherical accretion (dot-dashed line) and disk accretion (dashed line) for  $M_{\text{PBH}} = 10^3 M_{\odot}$  and  $f_{\text{PBH}} = 10^{-1}$ . For disk accretion, we have set the accretion parameter  $\lambda = 0.01$  and the radiative efficiency  $\epsilon = 0.1 \dot{m}$ . *Top panel.* The changes of the brightness temperature deviation,  $\Delta\delta T_b = \delta T_{b,\text{PBH}} - \delta T_b$ , with redshift  $z$ . *Bottom panel.* The gradient of the differential brightness temperature  $d\delta T_b/d\nu$  as a function of frequency  $\nu$ .

could reach at least  $\sim 15$  mK, have the ability to distinguish the global 21 cm signal impacted by accreting PBHs from that of the standard scenario. On the other hand, a detection of the gradient of the differential brightness temperature in the frequency range  $\nu \sim 20 - 40$  MHz with an amplitude smaller than  $\sim 1.8$   $\text{mK MHz}^{-1}$  will provide a possible evidence of accreting PBHs.

## 6 ACKNOWLEDGEMENTS

Y. Yang thanks Dr. Bin Yue and Fupeng Zhang for useful discussions. Y. Yang is supported in part by the Youth Innovations and Talents Project of Shandong Provincial Colleges and Universities (Grant No. 201909118)

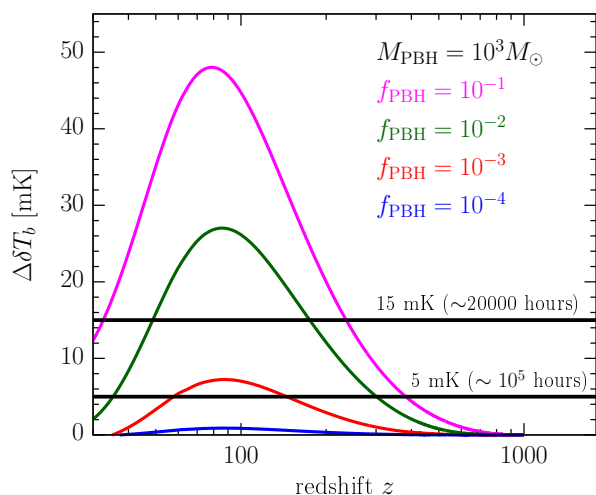


**Figure 4.** The brightness temperature deviation  $\Delta\delta T_b$  for different mass fraction of PBHs with  $M_{\text{PBH}} = 10^3 M_{\odot}$  for the disk accretion scenario. The horizontal lines show the uncertainty of  $\delta T_b$  ( $1\sigma$ ), 5 mK and 15 mK, which could be achieved by  $\sim 10^5$  and  $\sim 20000$  hours observation of future radio telescope (Burns 2020; Rapetti et al. 2020).

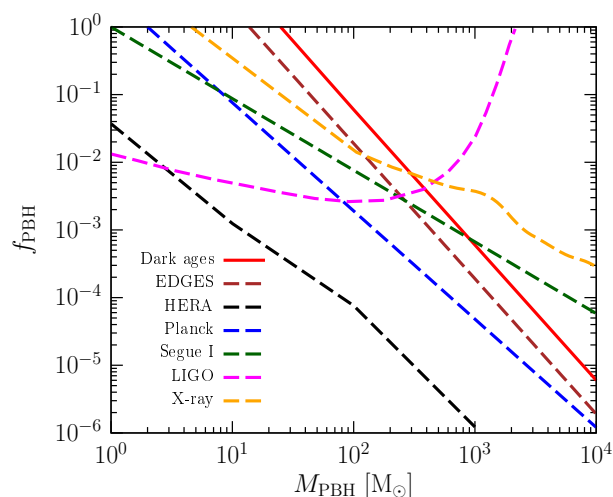


**Figure 5.** Upper limits on the mass fraction of PBHs for future observation of the 21 cm signal in the dark ages for the disk accretion scenario (red solid line, labelled with dark ages). For comparison, the constraints from a few other studies are also shown (dashed lines in different colors): 1) constraints from the observation of the global 21 cm signal in the cosmic dawn by EDGES (brown line, labelled with EDGES) (Hektor et al. 2018); 2) future detection of the 21 cm power spectrum in the cosmic dawn by HERA (black line, labelled with HERA) (Mena et al. 2019); 3) constraints from the CMB using the Planck data (blue line, labelled with Planck) (Poulin et al. 2017); 4) the influences of PBHs on the dynamical evolution of stars in dwarf galaxy Segue I (green line, labelled with Segue I) (Koushiappas & Loeb 2017); 5) non-detection of the stochastic GW background by LIGO (magenta line, labelled with LIGO) (Raidal et al. 2017); 6) investigation of the number density of X-ray objects in galaxies (orange line, labelled with X-ray) (Inoue & Kusenko 2017). Note that the region above each line is excluded by the corresponding study.

## 7 DATA AVAILABILITY

No new data were generated or analysed in support of this research.

## REFERENCES

- Agol E., Kamionkowski M., 2002, *Mon. Not. Roy. Astron. Soc.*, 334, 553
- Ali-Haïmoud Y., Kamionkowski M., 2017, *Phys. Rev.*, D95, 043534
- Barkana R., 2018, *Nature*, 555, 71
- Barkana R., Outmezguine N. J., Redigolo D., Volansky T., 2018, *Phys. Rev.*, D98, 103005
- Belotsky K. M., Kirillov A. A., 2015, *JCAP*, 1501, 041
- Berlin A., Hooper D., Krnjaic G., McDermott S. D., 2018, *Phys. Rev. Lett.*, 121, 011102
- Bertone G., Hooper D., Silk J., 2005, *Phys. Rept.*, 405, 279
- Bhatt J. R., Mishra A. K., Nayak A. C., 2019, *Phys. Rev.*, D100, 063539
- Bird S., Cholis I., Muñoz J. B., Ali-Haïmoud Y., Kamionkowski M., Kovetz E. D., Raccanelli A., Riess A. G., 2016, *Phys. Rev. Lett.*, 116, 201301
- Blas D., Lesgourgues J., Tram T., 2011, *Journal of Cosmology and Astroparticle Physics*, 2011, 034
- Bondi H., 1952, *Mon. Not. Roy. Astron. Soc.*, 112, 195
- Bondi H., Hoyle F., 1944, *Mon. Not. Roy. Astron. Soc.*, 104, 273
- Bowman J. D., Rogers A. E. E., Monsalve R. A., Mozdzen T. J., Mahesh N., 2018, *Nature*, 555, 67
- Burns J. O., 2020, *Phil. Trans. R. Soc. A.*, 379, 20190564
- Burns J., et al., 2019, *BAAS*, 51, 6
- Burns J., et al., 2021, arXiv e-prints, p. arXiv:2103.05085
- Cai R.-G., Ding Y.-C., Yang X.-Y., Zhou Y.-F., 2021, *J. Cosmology Astropart. Phys.*, 2021, 057
- Cang J., Gao Y., Ma Y.-Z., 2021, *J. Cosmology Astropart. Phys.*, 2021, 051
- Carr B. J., Kohri K., Sendouda Y., Yokoyama J., 2010, *Phys. Rev. D*, 81, 104019
- Carr B., Kohri K., Sendouda Y., Yokoyama J., 2020, arXiv e-prints, p. arXiv:2002.12778
- Chen X., Kamionkowski M., 2004, *Phys. Rev. D*, 70, 043502
- Chen X., et al., 2019, in *ISSI-BJ Forum: Discover the Sky by Longest Wavelength with Small Satellite Constellation*. (arXiv:1907.10853)
- Ciardi B., Madau P., 2003, *Astrophys. J.*, 596, 1
- Clark S., Dutta B., Gao Y., Ma Y.-Z., Strigari L. E., 2018, *Phys. Rev.*, D98, 043006
- Cohen A., Fialkov A., Barkana R., Lotem M., 2017, *Mon. Not. Roy. Astron. Soc.*, 472, 1915
- Cumberbatch D. T., Lattanzi M., Silk J., Lattanzi M., Silk J., 2010, *Phys. Rev.*, D82, 103508
- D’Amico G., Panci P., Strumia A., 2018, *Phys. Rev. Lett.*, 121, 011103
- De Luca V., Franciolini G., Pani P., Riotto A., 2020, *Phys. Rev. D*, 102, 043505
- De Luca V., Franciolini G., Riotto A., 2021a, *Phys. Rev. Lett.*, 126, 041303
- De Luca V., Desjacques V., Franciolini G., Pani P., Riotto A., 2021b, *Phys. Rev. Lett.*, 126, 051101
- Feng C., Holder G., 2018, *Astrophys. J.*, 858, L17
- Furlanetto S., Oh S. P., Briggs F., 2006, *Phys. Rept.*, 433, 181
- Halder A., Banerjee S., 2021, *Phys. Rev. D*, 103, 063044
- Hasinger G., 2020, *JCAP*, 07, 022
- Hektor A., Hütsi G., Marzola L., Raidal M., Vaskonen V., Veermäe H., 2018, *Phys. Rev.*, D98, 023503

- Hoyle F., Lyttleton R. A., 1939, [Math. Proc. Cambridge Philos. Soc.](#), **35**, 405
- Hoyle F., Lyttleton R. A., 1940a, [Math. Proc. Cambridge Philos. Soc.](#), **36**, 325
- Hoyle F., Lyttleton R. A., 1940b, [Math. Proc. Cambridge Philos. Soc.](#), **36**, 424
- Inoue Y., Kusenko A., 2017, [JCAP](#), 1710, 034
- Jia L.-B., Liao X., 2019, [Phys. Rev. D](#), **100**, 035012
- Jungman G., Kamionkowski M., Griest K., 1996, [Phys. Rept.](#), **267**, 195
- Kohri K., Terada T., 2021, [Phys. Lett. B](#), **813**, 136040
- Koushiappas S. M., Loeb A., 2017, [Phys. Rev. Lett.](#), **119**, 041102
- Kovetz E. D., Cholis I., Kaplan D. E., 2019, [Phys. Rev.](#), **D99**, 123511
- Kuhlen M., Madau P., Montgomery R., 2006, [Astrophys. J.](#), **637**, L1
- Liszt H., 2001, [Astron. Astrophys.](#), **371**, 698
- Madhavacheril M. S., Sehgal N., Slatyer T. R., 2014, [Phys. Rev.](#), **D89**, 103508
- Mena O., Palomares-Ruiz S., Villanueva-Domingo P., Witte S. J., 2019, [Phys. Rev.](#), **D100**, 043540
- Mittal S., Ray A., Kulkarni G., Dasgupta B., 2021, arXiv e-prints, [p. arXiv:2107.02190](#)
- Page D. N., 1976a, [Phys. Rev. D](#), **13**, 198
- Page D. N., 1976b, [Phys. Rev. D](#), **14**, 3260
- Page D. N., 1977, [Phys. Rev. D](#), **16**, 2402
- Poulin V., Serpico P. D., Calore F., Clesse S., Kohri K., 2017, [Phys. Rev.](#), **D96**, 083524
- Pritchard J. R., Loeb A., 2012, [Rept. Prog. Phys.](#), **75**, 086901
- Raidal M., Vaskonen V., Veermäe H., 2017, [JCAP](#), **09**, 037
- Rapetti D., Tauscher K., Mirocha J., Burns J. O., 2020, [ApJ](#), **897**, 174
- Ricotti M., 2007, [Astrophys. J.](#), **662**, 53
- Ricotti M., Ostriker J. P., Mack K. J., 2008, [Astrophys. J.](#), **680**, 829
- Shapiro S. L., Lightman A. P., 1976, [ApJ](#), **204**, 555
- Slatyer T. R., 2016, [Phys. Rev.](#), **D93**, 023521
- Stöcker P., Krämer M., Lesgourgues J., Poulin V., 2018, [JCAP](#), **1803**, 018
- Tashiro H., Sugiyama N., 2013, [Mon. Not. Roy. Astron. Soc.](#), **435**, 3001
- Villanueva-Domingo P., Mena O., Miralda-Escudé J., 2020, [Phys. Rev. D](#), **101**, 083502
- Xu Y., Yue B., Chen X., 2021, arXiv e-prints, [p. arXiv:2102.12865](#)
- Yang Y., 2015, [Phys. Rev.](#), **D91**, 083517
- Yang Y., 2016, [Eur. Phys. J. Plus](#), **131**, 432
- Yang Y., 2018, [Phys. Rev.](#), **D98**, 103503
- Yang Y., 2019, [Mon. Not. Roy. Astron. Soc.](#), **486**, 4569
- Yang Y., 2020, [Phys. Rev. D](#), **102**, 083538
- Yuan F., Narayan R., 2014, [Ann. Rev. Astron. Astrophys.](#), **52**, 529
- Yuan Q., Yue B., Bi X.-J., Chen X., Zhang X., 2010, [JCAP](#), **1010**, 023
- Zhang L., Chen X., Kamionkowski M., Si Z.-g., Zheng Z., 2007, [Phys. Rev. D](#), **76**, 061301